High-precision drop shape analysis on inclining flat surfaces: Introduction and comparison of this special method with commercial contact angle analysis

ARTICLE *in* THE JOURNAL OF CHEMICAL PHYSICS · OCTOBER 2013

Impact Factor: 2.95 · DOI: 10.1063/1.4822261 · Source: PubMed

2 AUTHORS:

Michael Schmitt
Universität des Saarlandes
27 PUBLICATIONS **90** CITATIONS
SEE PROFILE

Florian Heib
Universität des Saarlandes
15 PUBLICATIONS **48** CITATIONS
SEE PROFILE

AIP | The Journal of Chemical Physics

High-precision drop shape analysis on inclining flat surfaces: Introduction and comparison of this special method with commercial contact angle analysis

Michael Schmitt and Florian Heib

Citation: The Journal of Chemical Physics **139**, 134201 (2013); doi: 10.1063/1.4822261
View online: http://dx.doi.org/10.1063/1.4822261
View Table of Contents: http://scitation.aip.org/content/aip/journal/jcp/139/13?ver=pdfcov
Published by the AIP Publishing

High-precision drop shape analysis on inclining flat surfaces: Introduction and comparison of this special method with commercial contact angle analysis

Michael Schmitt[a] and Florian Heib
Physical Chemistry, Saarland University, 66123 Saarbrücken, Germany

(Received 24 May 2013; accepted 11 September 2013; published online 4 October 2013)

Drop shape analysis is one of the most important and frequently used methods to characterise surfaces in the scientific and industrial communities. An especially large number of studies, which use contact angle measurements to analyse surfaces, are characterised by incorrect or misdirected conclusions such as the determination of surface energies from poorly performed contact angle determinations. In particular, the characterisation of surfaces, which leads to correlations between the contact angle and other effects, must be critically validated for some publications. A large number of works exist concerning the theoretical and thermodynamic aspects of two- and tri-phase boundaries. The linkage between theory and experiment is generally performed by an axisymmetric drop shape analysis, that is, simulations of the theoretical drop profiles by numerical integration onto a number of points of the drop meniscus (approximately 20). These methods work very well for axisymmetric profiles such as those obtained by pendant drop measurements, but in the case of a sessile drop onto real surfaces, additional unknown and misunderstood effects on the dependence of the surface must be considered. We present a special experimental and practical investigation as another way to transition from experiment to theory. This procedure was developed to be especially sensitive to small variations in the dependence of the dynamic contact angle on the surface; as a result, this procedure will allow the properties of the surface to be monitored with a higher precession and sensitivity. In this context, water drops onto a 111 silicon wafer are dynamically measured by video recording and by inclining the surface, which results in a sequence of non-axisymmetric drops. The drop profiles are analysed by commercial software and by the developed and presented high-precision drop shape analysis. In addition to the enhanced sensitivity for contact angle determination, this analysis technique, in combination with innovative fit algorithms and data presentations, can result in enhanced reproducibility and comparability of the contact angle measurements in terms of the material characterisation in a comprehensible way. © *2013 AIP Publishing LLC*. [http://dx.doi.org/10.1063/1.4822261]

I. INTRODUCTION

Wetting and contact angle analysis is of the utmost importance in science and industry. The practical relevance of the sessile drop method is immense, for example, for adhesion[1] and in characterising of surfaces,[2,3] *exempli gratia*, surfaces coated by self-assembling monolayers[4] and surfaces with controlled topography.[5] Unfortunately, wetting experiments by simply applying drops onto surfaces are very critical in terms of the reproducibility, sensitivity, and precision of the determined apparent contact angle. The modern literature has been flooded with the publications presenting contact angles of questionable quality, including contact angles interpretation. Some researchers alarmed surface chemistry community on this problem in several publications over the last decade.[6] Many parameters with inexact or even unknown influences on the phase contacts (mainly liquid-vapour, solid-liquid-vapour) and, therefore, on the contact angle exist, such as gravity,[7] the relative position in the gravity field, the surface roughness and heterogeneities,[8–12] line tensions,[13] surface-liquid interactions, the drop size,[14] and the temperature.[15–17] Theoretical concepts are not sufficiently developed to include all of these effects, and forcing in commercial software routines can result in critical faults. Common software fits one circle/ellipse or some polynomial function (tangential) onto the drop shape. The procedures and fit-limits are not easily understood and are not controllable. Most of the procedures have fair reproducibility and precision. Theoretical drop shape simulations, particularly the *axisymmetric drop shape analysis*[18] based on numerical optimisation, are very suitable for pendant drop measurements and for flat ideal surfaces that are measured without inclination. Methods that are completely independent from theoretical concepts based on image software also exist.[19]

Our investigation is to develop a special rational technique based on theoretical aspects to determine, *inter alia*, the measured contact angle θ_m using the example of non-axisymmetric drops obtained by inclining a surface. In the presented work, an ideal flat chemical homogeneous surface will be under investigation. Therefore, a drop of 50 μl of ultra-pure water onto a 111 silicon wafer is dynamical analysed. This wafer was exposed to atmosphere after the fabrication so that spreading was not expected.[20] It is important that all of the limits and the parameters such as the

[a]mic.schmitt@mx.uni-saarland.de

length of the meniscus are controlled and taken into account so that higher sensitivity and precision in comparison to classical methods are obtainable. The developed technique, called high-precision drop shape analysis (HPDSA), will be able to independently and dynamically analyse both contact angles of a sequence/video of sessile drops so that non-axisymmetric analysis is possible. Within this publication, the concept of the technique is explained in detail. The obtained dynamic contact angles are compared with a standard fitting procedure of a modified OCA-contact angle system, which is also used to determine the video of the measurements.

II. BACKGROUND

The most important facts concerning the physical and physical-chemical concepts of the two- and tri-phase contacts taking place in every apparently simple wetting experiment are discussed within this section. This basic knowledge is essential to follow the operational steps of the HPDSA. These topics are explained in detail in textbooks.[1,21]

A. Theoretical basics

The thermodynamic system of a sessile drop in thermodynamic equilibrium contains more than just solid (s), vapour (v), and liquid (l) phases. The additional interfaces, solid-vapour, solid-liquid, liquid-vapour, and solid-liquid-vapour, are often not considered or are approximated as sharp transitions with a discontinuity in the physical properties.[22] This practice is a critical simplification, especially if the effects of the interface, such as surface tension and contact angles, are investigated. The exact mathematical description of the interphases is impossible due to discontinuities and the unknown thicknesses of the transition region. An approach is given by Gibbs and his dividing surface, *D-face*.[15,16,23] This approximation is based on the introduction of excess values, *exempli gratia*, the total amount (mol) $n_{total,\,i}$ of the compound i in two-phase-system α and β,

$$n_{total,i} = n_i^{\alpha} + n_i^{\beta} + n_{i;\alpha,\beta}^{D} \tag{1}$$

with n_i^{α} and n_i^{β} being the bulk amount of the substances and $n_{i;\alpha,\beta}^{D}$ being an excess value. As a function of the position of the *D-face* in relation to the amount of substance, this value is positive, zero, or even negative. The absolute absorption Γ_i^D is the excess amount of substance relative to the area of the *D-face A*. The thermodynamic model leads to the specific *free energy* of the interface $f_{\alpha,\beta}^{D}$ (J m^{-2}),

$$f_{\alpha,\beta}^{D} = \sigma_{\alpha,\beta}^{D} + \sum_i \mu_i \Gamma_i^D, \tag{2}$$

known as the surface or interface energy that correlates the energy with the surface tension $\sigma_{\alpha,\beta}^{D}$ plus the sum of the product of the chemical potential μ_i and the absolute absorption of every compound of the system. The product is not determined because the position of the *D-face* is unknown. The thermodynamic surface tension $\sigma_{\alpha,\beta}^{D}$, which is defined as the work of the formation of a new surface area, is correlated with the mechanical surface tension $\gamma_{\alpha,\beta}^{D}$, which is defined as an excess surface stress per unit surface area[15,24] As a result of Eq. (2), it is impossible, even in a one-compound system, to postulate that the surface energy is equal to the surface tension. In almost every contact angle measurement, at least two compounds are present; therefore, the determination of surface energies is *a priori* impossible. The solid considered within this study is a flat silicon wafer that has nearly no effect on the vapour phase and a very low solubility in the liquid phase of water. The liquid used for this investigation is ultrapure water so that the amount of addition species is reduced as far as possible. The two-phase interface with an enormous effect is the meniscus of liquid. The generalised *Laplace equation*,

$$\Delta p = \frac{\Delta F}{A} = \gamma_{\alpha,\beta}^{D}\left(\frac{1}{R_1} + \frac{1}{R_2}\right) - \frac{c_1}{R_1^2} - \frac{c_1}{R_2^2} + \Gamma^D \times g \times \cos\Phi, \tag{3}$$

describes the relation of the difference in the pressures Δp, that is, in the forces ΔF per area A, between the two phases with interfacial tensions $\gamma_{\alpha,\beta}^{D}$, principal radii of curvature R_i, curvature constants c_i, absolute absorption Γ^D, a gravity acceleration g, and an angle Φ relative to the gravitation field. For the tri-phase solid-liquid-vapour contact, which is known as the triple line or, due to the 2D-projection of 3D-object, as the triple point, in 1804, Young published one of the most well-known equations that correlates the mechanical surface tensions with the equilibrium contact angle θ_e in a thermodynamic and mechanical equilibrium:

$$\gamma_{s,v} = \gamma_{s,l} + \gamma_{l,v} \times \cos\theta_e. \tag{4}$$

Especially for solids with large mechanic moduli, additional parameters such as the line tension are negligible. To also exclude the line-tension effects, large drops[14] with 0.05 ml volumes corresponding to ~8 mm diameters are used in this investigation.

B. Practical aspects

Apparent contact angles are determined as the angles between the solid-liquid and solid-vapour interfaces, *exempli gratia*, from drops after simply applying the liquid onto the surface. In this way, neither any comparable contact angle nor the thermodynamic equilibrium contact angle θ_e are determined. However, even if no effect of the surface exists, only the macroscopic artefact of the thermodynamic contact angle is obtained due to the macroscopic tangent on the liquid-vapour interphase. Nevertheless, the macroscopic determination of such apparent contact angles from sessile drops is regularly published without even a consideration of the additional effects or without referring to important parameters such as the measurement procedure, the tilting angle, the temperature, the volume, both compounds, the surface roughness, the heterogeneity, and the phases. Scientific investigations clearly demonstrate that, in particular, the roughness, the temperature, the vapour, and the volume influence the contact angle.[25] Therefore, all experiments of this investigation are performed with controlled temperature and atmosphere. For

example, the surface roughness results in a huge difference between the advancing contact angle $\theta_{a,e}$, which corresponds to the angle measured after the triple line advanced onto an area that was not previously wetted, and the receding contact angle $\theta_{r,e}$, which corresponds to the angle measured after the triple line receded onto a previously wetted area.[26] For the sake of completeness, both angles are sometimes also defined as the angles measured before the triple line shows this jumping motion or are even determined at defined inclination angles. Unfortunately, not all authors clearly defined the used definition. The difference between the two angles is known as the contact angle hysteresis $\Delta\theta$,[12] whose existence is often mainly attributed to the surface roughness. In particular, the influence of gravity (due to factors like changing distribution of the weight force on the triple line) and other variations on the two-phase interface of the drop are not studied in detail for sessile drop experiments. Due to different changes in the position relative to the gravity field, compared to Eq. (3), advancing θ_a and receding θ_r must differ from the downhill angle θ_d and the uphill angle θ_u, which are measured by the inclined surface and will also be functions of the tilting angle in a complex combination with the surface roughness. In this study an ideal flat silicon oxide surface is used to reduce surface roughness dependent contact angle hysteresis. To investigate all these points, adequate software working with rational theories do not exist, are not well-known, or have not been available until now.

III. EXPERIMENTAL

A. Materials

The test liquid water was produced by a Milli-Q® Type 1 ultrapure water system, Merck KGaA, Darmstadt, Deutschland. The polished p-type 111 silicon wafer was provided by Siltronic AG, München, Germany, and was cleaned by successive rinsing with pure hexane, ethanol, and isopropanol before the experiment. The surface roughness was in the regime of 10^0 nm; therefore, the effects of the roughness would not dominate the contact angle measurements. The wafer was exposed to air after the fabrication. A strong suggestion exists that the surface was well passivized by the formed thin film of oxide and would not react with the water.

B. Measurement

An OCA20-contact angle measuring system, dataphysics, Filderstadt, Germany, was used to record the changes and movements (resolution 768 × 574 pixel; 12.5 images/second) of the 0.05 ml drop during the inclining of the surface with 0.943°/s ± 0.005°/s. The OCA-equipment tilts to the right-hand side. A modified measuring chamber was utilised, which was closed so that the liquid could be measured in thermodynamic equilibrium with its vapour, 100% atmospheric humidity (moist air atmospheric pressure 1 bar) at temperature 29.7 °C, which was kept constant by a Lauda ecoline control head E100 and a cryothermostat RE194, Lauda Dr. R. Wobser GmbH and co. KG, Lauda-Königshofen, Germany. The vapour was saturated by additional drops during a 2 h dwell time at the temperature. In addition to the "ellipse fitting" analysis of the drop profile, the measurement was saved as an avi-video file.

C. From image to coordinates

The first step in the drop shape analysis is the extraction of the drop contour from the data (image or video). Of course, this extraction can be performed picture-by-picture by image analysis software, but a major aspect of our investigations is to maintain control and traceability of the procedure. Therefore, we decided to use a rational mathematical approach that will result in Cartesian coordinates, even at sub-pixel resolutions, independent from any image analysis software or even programming library. For this study, the technique is implemented in a c-based software, which is independent from other main software. The OCA-system produces an avi-file, which is convertible into loss-free bmp images by a program such as the freeware program virtualdub v1.9.11 1998-2010 by Avery Lee. For every pixel, the bmp format contains three hexadecimal numbers between "00" and "ff" (decimal 0 and 255) that correspond to the *RGB* colour. Hence, the sum of the decimal colour values *col* ranges from 0 (black) to 765 (white). The successive automatic read-out of the data and analysis of the pixel colours are performed by the c-based software. During this process, a pixel-to-length transformation with 54.6 pixels/mm takes place due to the used magnification of the OCA-system. The direction of the *Cartesian* coordinate system is rationally defined from the bottom to the top as the *x*-axis and from the left to the right of the image as the *y*-axis (to compare to Sec. III D). Dynamic linear regressions of the sum of the decimal colour values *col* of five $n = 5$, $P_i \in \{0, 1, 2, 3, 4\}$ and of three neighbouring pixels $n = 3$, $P_i \in \{0, 1, 2\}$ occur to calculate the rates of the colour $p_{x/y}$ for every pixel,

$$\left(\frac{d\,col}{d\,P}\right)_{x/y} = \frac{\sum (col_i \times P_i) \times n - \sum col_i \times \sum P_i}{n \times \sum P_i^2 - \left(\sum P_i\right)^2} = p_{x/y}, \tag{5}$$

where the considered pixel is No. 2 for a five-point regression and No. 1 for a three-point regression. This procedure takes place in two independent, orthogonal directions (axial, *y*-direction, p_{y_j}, and horizontal, *x*-direction, p_{x_j}). The software has implemented different procedures to reduce the reflections and noise within/of the images. For example, only pixels with rate values that significantly differ from zero in both regressions are considered suitable (Table II). Using the above procedure and implementing adjustable limits for the rates in the program code result in different numbers of *x*, *y*-points as shown in Figure 1 and Table I. This procedure must lead to at least two points for one step in colour. Thus, for every colour step, a weighting procedure in the horizontal or vertical direction is reasonable, which is based on the rates p_{x_j}, p_{x_j}, and p_{y_j},

$$E(x) = \frac{\sum (x_j \times p_{x_j})}{\sum p_{x_j}} \quad \text{and} \quad E(y) = \frac{\sum (y_j \times p_{y_j})}{\sum p_{y_j}}, \tag{6}$$

resulting in the expectancy values $E(x)$ and $E(y)$. The standard

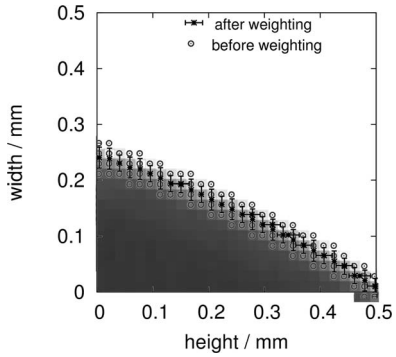

FIG. 1. Superposition of the drop image with the calculated coordinates before and after the weighting procedure. The image is converted into coordinates with a sub-pixel resolution. In this figure, the surface of the solid corresponds to the *y*-axis due to the rotation of the coordinates and the definition of the bmp format.

deviations $\sigma(x)$ and $\sigma(y)$ are also computable:

$$\sigma(x)=\sqrt{\sum\left(\frac{p_{x_j}}{\sum p_{x_j}}(x_j-E(x))^2\right)}, \tag{7}$$

$$\sigma(y)=\sqrt{\sum\left(\frac{p_{y_j}}{\sum p_{y_j}}(y_j-E(y))^2\right)}. \tag{8}$$

As a result, the drop shape is converted into coordinates with a sub-pixel resolution, Figure 1.

D. Fitting on the drop shape

The data points obtained by the technique in Sec. III C are basing on *x, y*-coordinates; therefore, common data analysis and graphing software such as OriginLab or Microsoft Excel and every function are possible for least-square fitting procedure. According to theory, especially to the *Laplace* equation, Eq. (3), the curvature of every single point of the drop meniscus is of interest; therefore, a circle is a rational function to examine the radius R being one radius of curvature,

$$y_{1/2}(x) = y_{CC} \pm \sqrt{R^2-(x-x_{cc})^2}, \tag{9}$$

TABLE I. Example for colour rates in bmp-images. The 5-point regression is less sensitive to noise (Nos. 8 and 10) but less specific to the position (Nos. 2 and 5).

Number	Sum of colour value	Rate of the 5 points regression	Rate of the 3 points regression
1	765	0.0	0.0
2	765	– 153.0	0.0
3	765	– 229.5	– 382.5
4	0	– 229.5	– 382.5
5	0	– 153.0	0.0
6	0	0.0	0.0
7	0	80.4	0.0
8	0	40.2	201.0
9	402	0.0	0.0
10	0	– 40.2	– 201.0
11	0	– 80.4	0.0
12	0	0.0	0.0

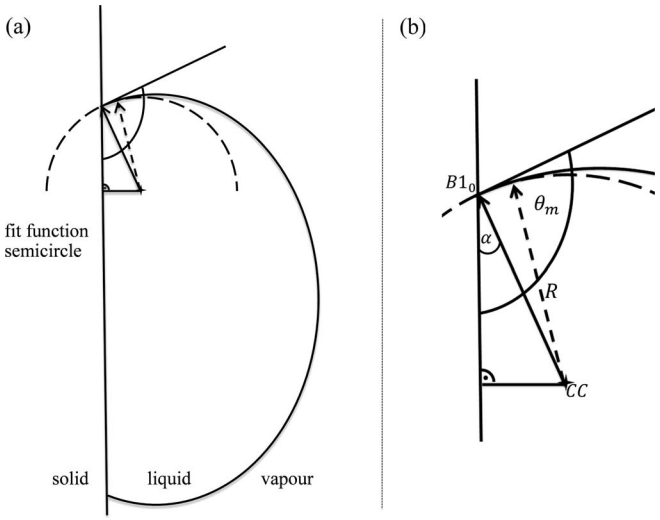

FIG. 2. Illustration of the fitting of a semicircle (dashed) on the drop shape rotated by 90° (a). Definition and calculation of the measured contact angle is visualised on the left (b).

where the coordinates x_{CC}: y_{CC} define the centre of a fitting circle *CC*. A circle is not one but two functions $y_1(x)$ and $y_2(x)$, a combination of two semicircles. Hence, to be able to calculate contact angles larger than 90°, an exchange in coordinate axis takes place in this study (Figure 2). Without this exchange, a contact angle of 90° will result in a rate tending towards ±infinity. By this procedure, the drop is also separated into a left (bottom) and a right half (top), which can be independently fitted by semicircles. The freeware program gnuplot v.4.6 1986-2012 by Williams, Kelley, and many others is used in our case for the fitting procedure, which takes place until the change in the sum of the squared differences is smaller than 10^{-20}. The main advantage of the program gnuplot is that the control files are text based and therefore dynamically writeable. Thus, for every drop shape, sets of boundary points and starting subroutines for the automatically fitting procedure are created.

Therefore, the minimal length of a calculation arc of the circle l_{arc},

$$l_{arc} = \sqrt{(y_{B1}-y_{B2})^2+(x_{B1}-x_{B2})^2}, \tag{10}$$

is 500 μm in this publication so that the c-based program is able to calculate the boundary points of the fitting procedure $B1$ with x_{B1}: y_{B1} and $B2$ with x_{B2}: y_{B2} starting with the triple-point $B1_0$ with x_{B1_0} : y_{B1_0}. For the used software, the second set of boundary points has a two-thirds overlap with the first one and so on. The meniscus to be fitted is also 500 μm for this publication. After the automatic fitting procedure, the real length of the arc of every circle b_{arc} can be calculated:

$$b_{arc} = 2\pi \times R \times \frac{\beta_{arc}}{360^\circ}, \tag{11}$$

where β_{arc} is the angle between the vectors $\vec{d}_{B1:CC}$ and $\vec{d}_{B2:CC}$. This angle is obtainable by the cosine theorem:

$$d_{arc}{}^2 = |\vec{d}_{B1:CC}|^2 + |\vec{d}_{B2:CC}|^2 - 2|\vec{d}_{B1:CC}||\vec{d}_{B2:CC}|^2 \times \cos\beta_{arc} \tag{12}$$

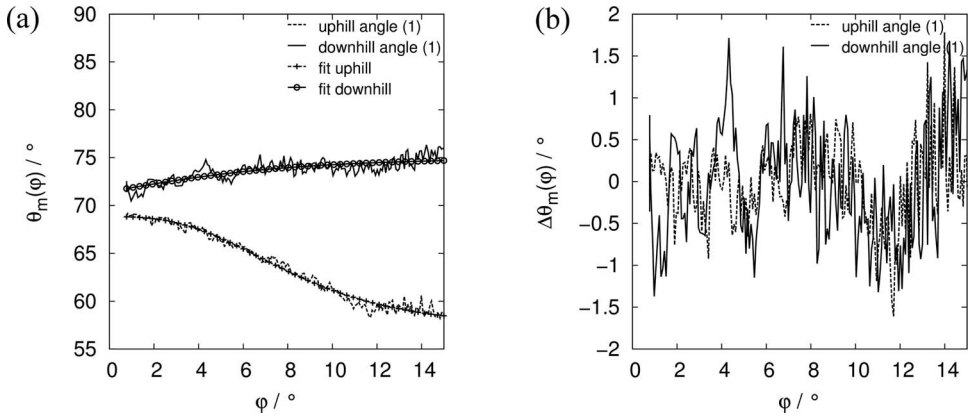

FIG. 3. Left (a) $\theta_m(\varphi)$ determined by HPDSA for the results of one measuring position in a clear decrease of the downhill angles and a smaller increase of the uphill angles. Fit functions, in general, have very good correlations with the course of the uphill and downhill angle; Right (b) The residuals $\Delta\theta_m(\varphi) = \theta_m(\varphi) - f(\varphi)$ relative to modified *Gompertzian* functions $f(\varphi)$ seem to be slightly disturbed. A correlation between the uphill and downhill angles is clearly visible.

with the length of the vectors equal to R. For further investigations, *inter alia*, the distance $b_{surface}$ between the surface $x_{B1_0} : y_{1/2}(x_{B1_0})$ and the centre of every calculation arc is computable similar to the distances and angles above:

$$b_{surface} = 2\pi \times R \times \frac{\beta_{total}}{360^\circ} = 2\pi \times R \times \frac{0.5\beta_{arc} + \beta_{sur}}{360^\circ}, \tag{13}$$

$$\beta_{sur} = \text{acos}\left(\frac{|\vec{d}_{B1:B1_0}|^2 - 2R2}{-R^2}\right). \tag{14}$$

In the future, this total length of the arc of a cycle $b_{surface}$ will be interesting to correlate from the radii of curvature to the distance of the solid-liquid interactions and the gravitational influences on the liquid-vapour interface. Finally, the calculation of the contact θ_m takes place not by some tangent on the triple point but by the sine theorem in a right-angled triangle (Figure 2):

$$\theta_m = 90^\circ + \alpha = 90^\circ + a \sin\left(\frac{x_{cc} - x_{B1_0}}{R}\right). \tag{15}$$

The software basing on this technique is additionally able to determine the drop diameter, the velocity of the boundary points by a three-point linear regression, the contact angle hysteresis, the time and inclining angle calculation, and the correction of the baseline if either the camera or the sample desk is not absolutely horizontal in the beginning of the measurement.

IV. RESULTS

A. Contact angle obtained by high-precision drop shape analysis

The measured contact angles $\theta_m(\varphi)$ were obtained as functions of the inclining angle φ by the described technique and software routine at six measuring positions from the experiments explained in Sec. III B. For the data processing of the measurements with inclining surfaces, the angles determined at the left half of the drop are called uphill angles and the angles at the right half are called downhill angles. For this publication, only the first calculation arc of a circle is considered with a (minimal) arc length of 500 μm. The first result was that the HPDSA parameter processing results in the detection of an initial inclination of the sample desk with approximately 1.64 pixels per 100 pixels, which is automatically corrected for the drop shape detection and also for the contact angle determination. The resulting plots of the contact angles $\theta_m(\varphi)$ have a clear decrease of the downhill angles and a smaller increase of the uphill angles (Figure 3 left).

For averaging and simple comparison of the signal courses, a modified *Gompertzian* function,[27]

$$f(\varphi) = \theta_{shift} + A \times \exp(-\exp(-k(\varphi - \varphi_{shift}))), \tag{16}$$

is fitted where θ_{shift}, A, k, and φ_{shift} are fitting parameters (Tables II and III). The drop is already running at the fit limit with an inclination angle $\varphi_{\max}$ of 15°. The residuals, $\Delta\theta_m(\varphi)$,

$$\Delta\theta_m(\varphi) = \theta_m(\varphi) - f(\varphi), \tag{17}$$

TABLE II. Data of the fitting of sessile drop measurements for the uphill angle calculated by HPDSA ($V = 0.05$ ml, $T = 29.7$ °C, inclining rate of 0.943°/s).

No.	θ_{shift} (°)	A (°)	k ($^{\circ -1}$)	φ_{shift} (°)	$f(0^\circ) = \theta_{u_i}^{50}$[a] (°)	$f(11^\circ) = \theta_u^{50}(11^\circ)$[a] (°)
1	68.88	−11.46	0.282	6.68	68.9	60.4
2	69.29	−24.60	0.085	8.94	66.4	58.7
3	69.53	−19.32	0.129	8.11	68.4	59.8
4	71.38	−21.79	0.134	8.57	70.4	60.8
5	68.02	−12.40	0.241	7.27	68.0	59.8
6	68.89	−12.27	0.236	7.25	68.8	60.8

[a]The superscript "50" corresponds to the drop volume in μl.

TABLE III. Data of the fitting of sessile drop measurements for the downhill angle calculated by HPDSA ($V = 0.05$ ml, $T = 29.7\,^{\circ}$C, inclining rate of 0.943°/s).

No.	θ_{shift} (°)	A(°)	k ($^{\circ -1}$)	φ_{shift} (°)	$f(0^{\circ}) = \theta_{d_i}^{50}$[a] (°)	$f(11^{\circ}) = \theta_{d}^{50}(11^{\circ})$[a] (°)
1	69.41	5.53	0.204	0.00	71.4	74.4
2	67.03	4.76	0.413	4.54	67.0	71.5
3	66.09	6.61	0.329	0.00	68.5	72.5
4	72.77	1.94	1.736	2.14	72.8	74.7
5	66.85	12.44	0.026	0.03	71.4	72.7
6	67.28	6.98	0.525	0.00	69.8	74.2

[a]The superscript "50" corresponds to the drop volume in μl.

for both the uphill and the downhill angles are in the regime of 1° and have similar deviations relative to their fit functions above inclinations of 8° when the drop is already running (Figure 3 right). The difference of 1.7° between the calculated initial average downhill angle $\langle\theta_{d_i}^{50}\rangle$ and the uphill angle $\langle\theta_{u_i}^{50}\rangle$ (Tables II and III) results most likely from the initial inclination of the sample desk and/or indicate that the camera itself could be slightly inclined. This difference is also in accordance with the published static contact angle hysteresis.[28] Kissinger *et al.*, 1991,[29] measured the apparent contact angles of silicon wafers with different treatments and storing times and concluded that "hydrophilic surfaces have angles of approximately 0° to 6° and hydrophobic ones of 50° to 70°." This result is in accordance with our results. Extrand *et al.*, 1997,[26] determined by inclining some silicon wafer surfaces that $\theta_a = 56.6^{\circ}$ and $\theta_r = 42.1^{\circ}$; however, this determination was made without cleaning the wafer before measuring and only considering one inclination angle.

B. Contact angle obtained by ellipse fitting

The same measurements as investigated in Sec. IV A from the experiments explained in Sec. III B were analysed by the "ellipse fitting" routine. The used routine required a vertical baseline for automatic video analysis. Therefore, due to the initial inclination, the position of the contact angle determination was not exactly at the triple point. As explained in Sec. IV A, the sample desk was slightly inclined by $\varphi_{initial} = 0.73^{\circ} \pm 0.09^{\circ}$; therefore, an additional manual correction was applied:

$$\theta_m(\varphi) = \theta_m(\varphi_{old} + \varphi_{initial}) = \theta_{m,old}(\varphi_{old}) + a \times \varphi_{initial}, \tag{18}$$

where a is 1 for uphill angles and -1 for downhill angles resulting from geometrical considerations. Note that without the HPDSA, this inclination is difficult to observe. The *Gompertzian* function (Eq. (16)) is also suitable for the contact angles determined by "ellipse fitting" (Figure 4), resulting in fitted courses that are similar to those of the HPDSA. In addition, the overall course of the residuals is similar to that of the HPDSA (Figures 3 and 4 right). The difference of -2.2° between the calculated initial average downhill angle $\langle\theta_{d_i}^{50}\rangle$ and uphill angle $\langle\theta_{u_i}^{50}\rangle$, Tables IV and V, is most likely an artefact of the detected initial inclination, see above.

V. DISCUSSION

A. High-precision drop shape analysis: Analysis of the residuals

The common definitions of *advancing* and *receding angles* are based on a visual detection of a movement of the triple line by a human eye. Even if video recording is possible, this approach is rational because the courses of downhill and uphill angles obtained, *exempli gratia*, by "ellipse fitting" (Figure 4) are sufficiently smooth that no specific point is definable. To prove the correlation between the fluctuations

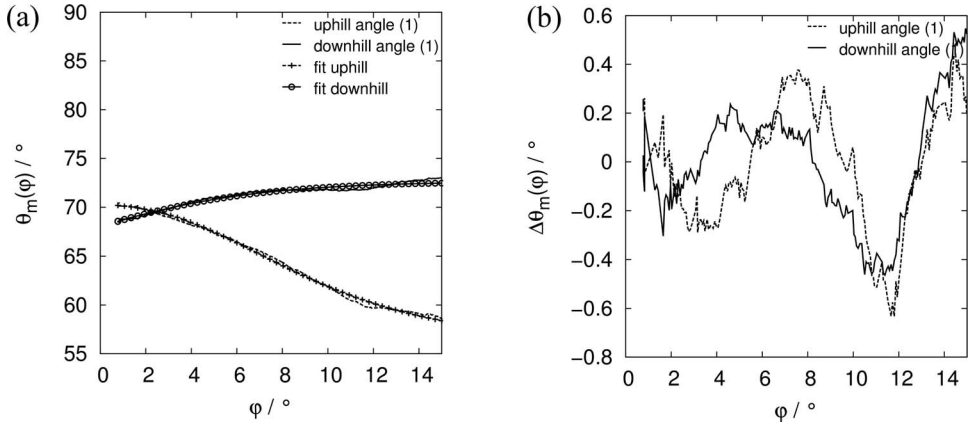

FIG. 4. Left (a) Inclination corrected $\theta_m(\varphi)$ calculated by an "ellipse fitting" method for one measuring position results in a clear decrease of the downhill angles and a smaller increase of the uphill angles. Right (b) The residuals $\Delta\theta_m(\varphi) = \theta_m(\varphi) - f(\varphi)$ relative to modified Gompertz function $f(\varphi)$ are without specific reflexes.

TABLE IV. Data of the fitting of sessile drop measurements for the uphill angle calculated by "ellipse fitting" ($V = 0.05$ ml, $T = 29.7\,^{\circ}$C, inclining rate of 0.943°/s).

No.	θ_{shift} (°)	A (°)	k ($^{\circ -1}$)	φ_{shift} (°)	$f(0^{\circ}) = \theta_{u_i}^{50}$[a] (°)	$f(11^{\circ}) = \theta_{u}^{50}(11^{\circ})$[a] (°)
1	70.41	−14.16	0.226	7.01	70.3	61.0
2	69.76	−25.78	0.094	9.94	67.7	59.3
3	70.50	−20.32	0.136	8.24	69.6	60.3
4	69.67	−17.65	0.160	7.43	69.0	59.6
5	68.12	−13.99	0.218	6.68	67.9	58.7
6	71.54	−20.68	0.139	8.37	70.7	61.2

[a]The superscript "50" corresponds to the drop volume in μl.

of the residuals obtained by HPDSA (Figure 3 right) and the movement of the drop, the velocity analysis tool of the HPDSA software is suitable. As mentioned above, the velocity of the boundary point, which is the triple point $B1_0$ for the first calculation arc, is obtained by a three-point linear regression that is dependent from the inclination angle (the software also allows time and image number, among others). This procedure in combination with the restriction in the optical resolution leads to steps in the velocity distribution even in continuous motion. One of the small sharp steps with approximately 40×10^{-6} m/° such as that by M1 below a 2° inclination in Figure 5 corresponds to a movement of the boundary point of approximately 6×10^{-6} m, whereas the pixel distance is approximately 18×10^{-6} m. As illustrated in Figure 5 and Figure S1 in the supplementary material,[30] the correlations between the contact angle fluctuations and the motion of the triple point are clearly recognisable. In general, the uphill angles increase after the movement, which seems to be more of a step-by-step process, whereas the contact angle at the downhill side increases before the movement takes place. Furthermore, the inclination angle when the movement appears is not the same for the downhill and uphill motions, especially for small inclination angles; therefore, no direct correlation exists between specific uphill and downhill angles. Thus, the published advancing and receding angles measured at the same image of a drop contain a significant error. Continuous motion that is macroscopically visible generally occurs at inclination angles larger than 4° for downhill motion and at angles larger than 9° for uphill motion with the inclining rate of 0.943°/s. At these angles $\varphi_{u/d}$, the specific downhill θ_d and uphill angles θ_u,

$$\theta_{u/d} = \Delta\theta_m(\varphi_{u/d}) + f(\varphi_{u/d}), \tag{19}$$

can be calculated (Figure 5, Tables II and III, Eq. (16)).

The first/critical motion of the triple line generally occurs by inclination angles smaller than 2°, which is not visible with the human eye and is, therefore, not known in literature. An additional publication concerning the roughness effects on this type of motion is in progress and will be published soon in which motion is manually captured and angles are obtained by commercial software. Some further topics for investigations are the consideration, analysis, and extrapolation of more than the first calculation arc and the variation of the arc length, especially aiming for a smaller fluctuation of the measured contact angle.

B. Comparison between ellipse fitting and high-precision drop shape analysis

The **precision** of the determination of contact angles is very important in all aspects. Therefore, angles without a baseline correction $\theta_{m,\,old}(\varphi_{initial})$ (Eq. (18)) both for "ellipse fitting" and HPDSA are considered, which, as previously mentioned, are significantly different from each other (Figures 3 and 4). A time delay between the start of the video stream and the inclination of the sample desk exists, which results in a number of drops with the same inclination angle $\varphi_{initial}$. Without the inclination correction, the downhill and uphill angles obtained by "ellipse fitting" are nearly identical, $\Delta\theta = 0.29^{\circ}$, whereas the HPDSA results in a significant hysteresis, $\Delta\theta = 4.79^{\circ}$ (Table VI).

Manually measuring the angle is insufficiently precise; therefore, a superposition procedure explained in Figure 6 occurs. The downhill angle is significantly larger and is clearly visible (Figure 6 right); otherwise, the shape of the (downhill) drop would not be recognisable.

The **sensitivity** of a contact angle determination is especially important if real surfaces that are rough or even

TABLE V. Data of the fitting of sessile drop measurements for the downhill angle calculated "ellipse fitting" ($V = 0.05$ ml, $T = 29.7\,^{\circ}$C, inclining rate of 0.943°/s).

No.	θ_{shift} (°)	A (°)	k ($^{\circ -1}$)	φ_{shift} (°)	$f(0^{\circ}) = \theta_{d_i}^{50}$[a] (°)	$f(11^{\circ}) = \theta_{d}^{50}(11^{\circ})$[a] (°)
1	65.40	7.26	0.244	0.00	68.1	72.2
2	64.15	6.93	0.259	3.18	64.9	70.2
3	67.06	4.57	0.344	2.02	67.7	71.4
4	65.13	5.39	0.333	0.55	66.8	70.4
5	63.43	6.02	0.234	0.00	65.6	69.0
6	68.73	3.65	0.415	2.68	68.9	72.3

[a]The superscript "50" corresponds to the drop volume in μl.

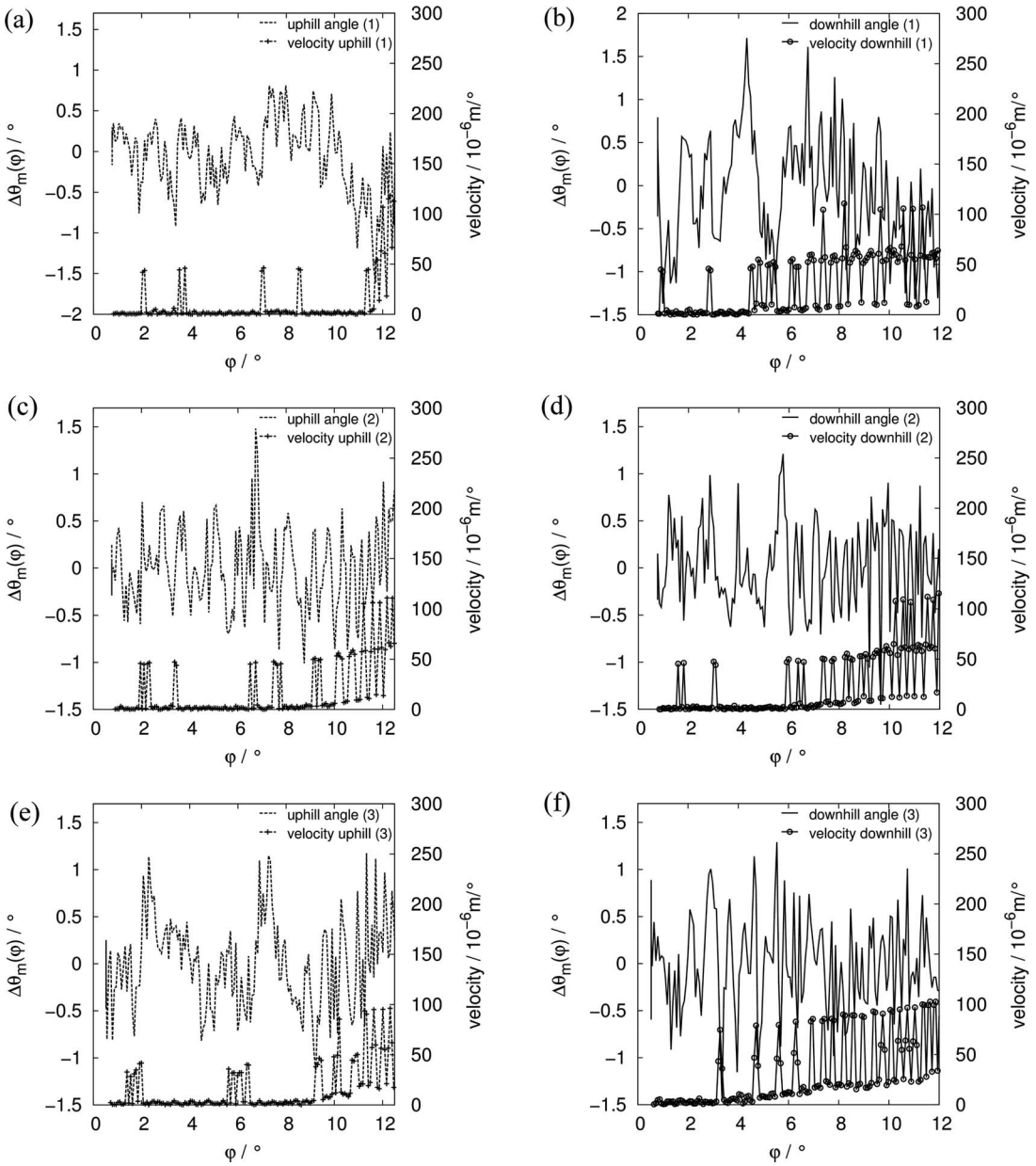

FIG. 5. Residuals $\Delta\theta_m(\varphi)$ and velocity of the position of the boundary point $B1_0$ from chosen measurements.

non-homogeneous are of interest. Additionally, for the definition of specific angles such as the advancing or the receding angle, sensitivity is important. Sensitivity-dependent relations between contact angle fluctuations by HPDSA and the velocity of the boundary points are clearly demonstrated within Sec. V A. Nevertheless, an additional verification of the higher sensitivity on the contact angle determination occurs. The measurement M5 with HPDSA results in a clearly

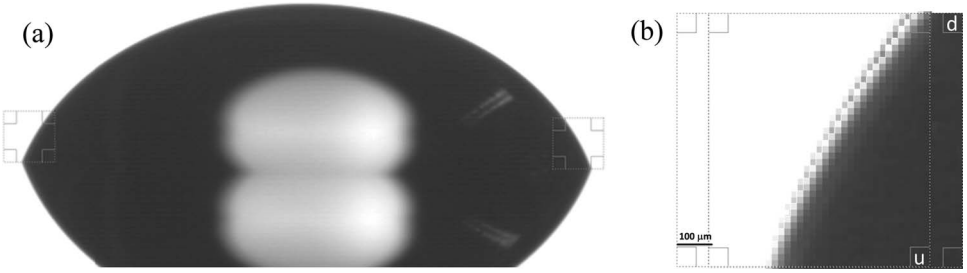

FIG. 6. Left (a) First image of the drop from measurement M1. Marked are the parts (40 × 40 pixel = 0.73 × 0.73 mm) for the superposition; Right (b) Superposition of the uphill (u) in the foreground and the mirrored downhill angle (d) in the background. The shape of the drop at the downhill side is visible; therefore, the downhill angle is significantly larger than the uphill angle.

TABLE VI. Average value of $\theta_{m,\,old}(\varphi_{initial})$ calculated from eleven images before the inclination starts analysed by HPDSA and "ellipse fitting."

	$\theta_{m,\,old}(\varphi_{initial})$ (°)
Downhill angle HPDSA	72.92
Uphill angle HPDSA	68.13
Downhill angle "Ellipse fitting"	69.64
Uphill angle "Ellipse fitting"	69.35

terminated reduction in the downhill contact angle value at inclination of ∼10.2°, whereas the "ellipse fitting" shows nothing (Figure 7 left).

This difference in contact angle is also provable by a superposition of the drop with $\varphi = 9.98°$ and the drop with $\varphi = 10.21°$ (Figure 7 right). A significant decrease in the contact angle is recognisable in the blown-up view due to the specific shift of the pixel colours.

The **reproducibility and comparability** of contact angle determination is especially important to characterise surfaces/materials. Therefore, it is rational to compare the fitted values for these 50 ml measurements, which are less effected by fluctuations, Tables II–V. The average contact angles for downhill $\langle\theta_d^{50}(\varphi)\rangle$ and uphill $\langle\theta_u^{50}(\varphi)\rangle$ analysed by "ellipse fitting" and HPDSA are shown in Figure 8.

Clearly visible is that the uphill angles, which decrease with increasing inclination, are nearly identical, whereas the downhill angles, which increase with increasing inclination, are different for "ellipse fitting" and HPDSA. The initial inclination $\varphi_{initial}$ that was detected only by the HPDSA results in the wrong position of the triple point for the downhill angle during the "ellipse fitting." Apart from this fault, the contact angles for downhill $\langle\theta_d^{50}(\varphi)\rangle$ and uphill $\langle\theta_u^{50}(\varphi)\rangle$ analysed by "ellipse fitting" and HPDSA are well correlated and comparable. The deviation of the contact angles is clearly reduced at inclinations larger than 8°. It would be welcome if contact angle measurements for smooth surfaces are published as

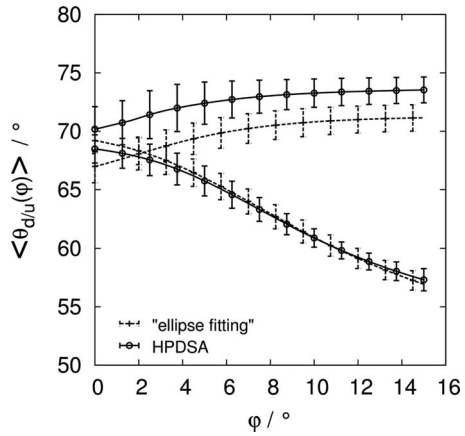

FIG. 8. Average downhill $\langle\theta_d^{50}(\varphi)\rangle$ (increasing) and uphill angles $\langle\theta_u^{50}(\varphi)\rangle$ (decreasing) and standard deviations at 29.7°C calculated by HPDSA and "ellipse fitting" from measurements at 6 positions. (Inclination with 0.973°/s and $V = 50\ \mu$l.)

presented in Figure 8 with volume and temperature always present. For the determination of the equilibrium contact angle θ_e the variation in the acting gravitational field and the movement of the drop in particular prevent any rational estimation. In addition, pinning and the inclination rate are aspects with unknown influences. All existing theories are not suitable; therefore, further investigations must occur.

VI. CONCLUSION

A high-precision drop shape analysis of sessile drops is introduced in detail, which can independently calculate the drop properties such as the dynamic contact angles and the radii of curvature above the drop meniscus for a sequence of images. For this publication, the technique is implemented in a c-program, the HPDSA software, to allow for automatic analysis of a sequence of images. The technique contains independent parts for the innovative pixel analysis, which allows the transformation of nearly every image (of a drop)

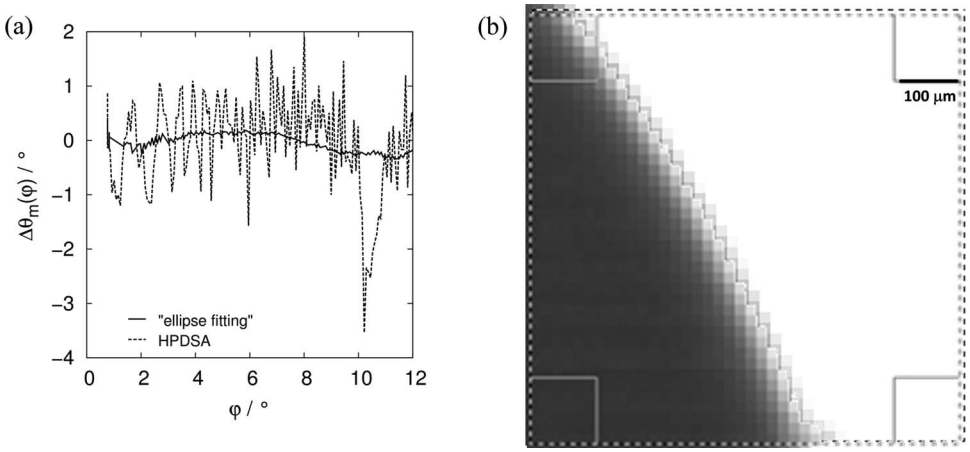

FIG. 7. Left (a) Residuals $\Delta\theta_m(\varphi)$ for the downhill angle of No. 5 calculated by HPDSA and "ellipse fitting." The HPSDA results in a decrease in θ_m between 9.98° and 10.21° of inclination φ; Right (b) Superposition of the same parts of the drop (position top left corner 580;333 pixel, 40 × 40 pixel = 0.73 × 0.73 mm) at 9.98° in the background and at 10.21° in the foreground. The second is shifted by 0.5 pixels to the left and bottom for the sake of the clarity. Note that the change in contact angle is real, $3.8° = \theta_m(9.98°) - \theta_m(10.21°) > f(9.98°) - f(10.21°) = 0.027°$, and is not simply an artefact, therefore, it is proven that the precision of HPDSA is enhanced. (Superposition of the fittings are shown in Figure S2 ("ellipse") and Figure S3 ("HPDSA")).

into coordinates with error estimations, and the consideration of the main radii, which results in the contact angle by geometric relationships and not by some tangent method. In the presented work, the contact angle is evaluated from *only the first* mean radii of curvature with a minimal length of the arc of 500 μm. Nevertheless, HPDSA has a much higher precision and is more sensitive to angle variations as the comparison of the contact angles by commercial "ellipse fitting" and by HPDSA clearly demonstrates. Therefore, definitions of a representative and reproducible advancing and receding or, if inclination takes place, of the uphill and downhill angle are possible, especially due to the determination of the velocity of the triple point. Our results also clearly prove that the uphill and downhill angles are not obtained by only analysing one image as was done in most of the published works because the movement is not correlated at the beginning of the moving. For smooth surfaces, the additional presented fitting method also usable with other determination techniques, resulting in courses for downhill and uphill angles that lead to an enhanced comparability in comparison with the estimation of some specific downhill and uphill angle. To our knowledge, an ideal flat surface like this flat silicon wafer has never before been characterised in such detail by contact angle measurements. Schmitt wants to share the ready-to-use programs and gnuplot-control files using the HPDSA-technique with every reader free of charge only for non-commercial use. The major aim is to improve the drop analysis, and he is looking forward to successful cooperation. Further investigations in terms of usability and data analysis will take place, *exempli gratia*, by increasing the number of considered calculation arcs and the variation of arc length, especially with the intention to analyse the local dependence of the curvature radius, which is impossible with any other method as far as we know. Due to the possibility of the software routine to independently analyse the contact angles and the radii of curvature, among others, data analysis obtained by another or modified hardware is possible and is not restricted to sessile drops. Especially interesting for the detection hardware is an increased resolution and magnification, which could experimentally improve understanding of the transition state between the meniscus and the surface/liquid film that is theoretically explained by Starov, 2013.[28] Exchanging the pure oxidised silicon surface with rough surfaces and surfaces resulting in higher or lower contact angles are additional points that will be investigated.

ACKNOWLEDGMENTS

The authors gratefully acknowledge R. Hempelmann for his support.

[1]L. F. M. da Silva, A. Oochsner, R. D. Adams, M. E. R. Shanahan, and W. Possart, *Handbook of Adhesion Technology - Wetting of Solids* (Springer-Verlag, Berlin, Heidelberg, 2011).

[2]I. Redsven, H. R. Kymalainen, E. Pesonen-Leinonen, R. Kuisma, T. Ojala-Paloposki, M. Hautala, and A. M. Sjoberg, Appl. Surf. Sci. **253**(12), 5536 (2007); R. S. Mane, C. D. Lokhande, V. V. Todkar, H. Chung, M. Y. Yoon, and S. H. Han, *ibid.* **253**(8), 3922 (2007); D. L. Schmidt, R. F. Brady, K. Lam, D. C. Schmidt, and M. K. Chaudhury, Langmuir **20**(7), 2830 (2004); N. Schwierz, D. Horinek, S. Liese, T. Pirzer, B. N. Balzer, T. Hugel, and R. R. Netz, J. Am. Chem. Soc. **134**(48), 19628 (2012).

[3]R. S. Faibish, W. Yoshida, and Y. Cohen, J. Colloid Interface Sci. **256**(2), 341 (2002).

[4]D. Khobragade, E. S. Stensrud, M. Mucha, J. R. Smith, R. Pohl, I. Stibor, and J. Michl, Langmuir **26** (11), 8483 (2010); Y. S. Obeng, M. E. Laing, A. C. Friedli, H. C. Yang, D. N. Wang, E. W. Thulstrup, A. J. Bard, and J. Michl, J. Am. Chem. Soc. **114**(25), 9943 (1992); E. Moore, D. O'Connell, and P. Galvin, Thin Solid Films **515**(4), 2612 (2006); M. A. Fox and M. D. Wooten, Langmuir **13**(26), 7099 (1997).

[5]D. Banerjee, S. Mukherjee, and K. K. Chattopadhyay, Carbon **48**(4), 1025 (2010); B. He, J. Lee, and N. A. Patankar, Colloids Surf., A **248**(1-3), 101 (2004); C. Bukowsky, J. M. Torres, and B. D. Vogt, J. Colloid Interface Sci. **354**(2), 825 (2011); J. W. Krumpfer and T. J. McCarthy, J. Am. Chem. Soc. **133**(15), 5764 (2011).

[6]J. Drelich, "Guidelines to measurements of reproducible contact angles using a sessile-drop technique," Surf. Innovations (published online).

[7]E. M. Blokhuis, Y. Shilkrot, and B. Widom, Mol. Phys. **86**(4), 891 (1995); C. A. Ward and M. R. Sasges, J. Chem. Phys. **109**(9), 3651 (1998).

[8]R. N. Wenzel, Ind. Eng. Chem. **28**, 988 (1936).

[9]N. K. Adam and G. E. P. Elliott, J. Chem. Soc. **1962**, 2206.

[10]A. B. D. Cassie and S. Baxter, Trans. Faraday Soc. **40**, 546 (1944).

[11]H. Kamusewitz and W. Possart, Appl. Phys. A: Mater. Sci. Process. **76**(6), 899 (2003).

[12]H. Kamusewitz, W. Possart, and D. Paul, Colloids Surf., A **156**(1-3), 271 (1999).

[13]D. Q. Li, Colloids Surf., A **116**(1-2), 1 (1996); A. Amirfazli, D. Y. Kwok, J. Gaydos, and A. W. Neumann, J. Colloid Interface Sci. **205**(1), 1 (1998).

[14]J. Drelich, J. Adhes. **63**(1-3), 31 (1997); J. Drelich, J. D. Miller, and R. J. Good, J. Colloid Interface Sci. **179**(1), 37 (1996).

[15]A. I. Rusanov, Surf. Sci. Rep. **23**(6-8), 173 (1996).

[16]A. I. Rusanov, Surf. Sci. Rep. **58**(5-8), 111 (2005).

[17]C. J. Budziak, E. I. Varghabutler, and A. W. Neumann, J. Appl. Polym. Sci. **42**(7), 1959 (1991).

[18]M. Hoorfar and A. W. Neumann, Adv. Colloid Interface Sci. **121**(1-3), 25 (2006); J. Adhes. **80**(8), 727 (2004); D. Li, P. Cheng, and A. W. Neumann, Adv. Colloid Interface Sci. **39**, 347 (1992).

[19]A. F. Stalder, G. Kulik, D. Sage, L. Barbieri, and P. Hoffmann, Colloids Surf., A **286**(1-3), 92 (2006).

[20]K. Hermansson, U. Lindberg, B. Hök, and G. Palmskog, in *Proceedings of the International Conference on Solid-State Sensors and Actuators Digest of Technical Papers (TRANSDUCERS'91)* (IEEE, 1991), pp. 193–196.

[21]A. W. Adamson and A. P. Gast, *Physical Chemistry of Surfaces*, 6th ed. (John Wiley and Sons, 1997); Y. H. Erbil, *Surface Chemistry - of Solid and Liquid Interfaces* (Blackwell Publishing, Oxford, 2006).

[22]P. Ehrenfest, Proc. Royal Acad. Amsterdam **36**, 153–157 (1933).

[23]J. W. Gibbs, Am. J. Sci. (Series 3) **16**, 441–458 (1878).

[24]B. V. Toshev and D. Platikanov, Colloids Surf., A **291**(1-3), 177 (2006).

[25]S. Cioulachtjian, S. Launay, S. Boddaert, and M. Lallemand, Int. J. Therm. Sci. **49**(6), 859 (2010).

[26]C. W. Extrand and Y. Kumagai, J. Colloid Interface Sci. **191**(2), 378 (1997).

[27]M. Schmitt, R. Schulze-Pillot, and R. Hempelmann, Phys. Chem. Chem. Phys. **13**(2), 690 (2011).

[28]V. Starov, Colloid Polym. Sci. **291**(2), 261 (2013).

[29]G. Kissinger and W. Kissinger, Phys. Status Solidi A **123**(1), 185 (1991).

[30]See supplementary material at http://dx.doi.org/10.1063/1.4822261 for a figure about the residuals $\Delta\theta_m(\varphi)$ and velocity of the position of the boundary point $B1_0$ from measurement 4 to 6 and additional figures concerning the fitting of "ellipse fitting" and "HPDSA."